Article

Biogenic Silver Nanoparticles Conjugated with Nisin: Improving the Antimicrobial and Antibiofilm Properties of Nanomaterials

Patricia Zimet [1], Ruby Valadez [2,3], Sofía Raffaelli [2], María Belén Estevez [2], Helena Pardo [1] and Silvana Alborés [2,*]

[1] Centro NanoMat, Facultad de Química, Instituto Polo Tecnológico de Pando, DETEMA, Universidad de la República, Montevideo 11800, Uruguay; pzimet@fq.edu.uy (P.Z.); hpardo@fq.edu.uy (H.P.)
[2] Área de Microbiología, Departamento de Biociencias, Facultad de Química, Universidad de la República, Montevideo 11800, Uruguay; 15030688@itcelaya.edu.mx (R.V.); sraffaelli@fq.edu.uy (S.R.); bestevez@fq.edu.uy (M.B.E.)
[3] Tecnológico Nacional de México en Celaya, Guanajuato 38010, Mexico
* Correspondence: salbores@fq.edu.uy; Tel.: +598-29244209

Abstract: Microbial technology offers a green alternative for the synthesis of value-added nanomaterials. In particular, fungal compounds can improve silver nanoparticle production, stabilizing colloidal nanoparticles. Based on a previous study by our group, silver nanoparticles obtained using the extracellular cell-free extracts of *Phanerochaete chrysosporium* (PchNPs) have shown antimicrobial and antibiofilm activity against Gram-negative bacteria. Moreover, nisin—a bacteriocin widely used as a natural food preservative—has recently gained much attention due its antimicrobial action against Gram-positive bacteria in biomedical applications. Therefore, the aim of this work was to conjugate biogenic silver nanoparticles (PchNPs) with nisin to obtain nanoconjugates (PchNPs@nis) with enhanced antimicrobial properties. Characterization assays were conducted to determine physicochemical properties of PchNPs@nis, and also their antibacterial and antibiofilm activities were studied. The formation of PchNPs@nis was confirmed by UV-Vis, TEM, and Raman spectroscopy analysis. Different PchNPs@nis nanobioconjugates showed diameter values in the range of 60–130 nm by DLS and surface charge values between −20 and −13 mV. Nisin showed an excellent affinity to PchNPs, with binding efficiencies higher than 75%. Stable synthesized PchNPs@nis nanobioconjugates were not only able to inhibit biofilm formation by *S. aureus*, but also showed inhibition of the planktonic cell growth of *Staphyloccocus aureus* and *Escherichia coli*, broadening the spectrum of action of the unconjugated antimicrobials against Gram-positive and Gram-negative bacteria. In conclusion, these results show the promising application of PchNPs@nis, prepared via green technology, as potential antimicrobial nanomaterials.

Keywords: biogenic nanoparticles; nanobioconjugates; nisin; antimicrobial; antibiofilm

1. Introduction

In the last years, biological synthesis of nanomaterials using microorganisms has shown immense potential as an ecofriendly and cost-effective alternative to traditional methods. Conventional physical and chemical methods used to synthetize nanoparticles may require the use of toxic reagents as well as severe and/or expensive reaction conditions, which may be harmful for human health and the environment. Green approaches are based on the utilization of natural products (from microorganisms or plants) as reducing and stabilizing agents for the synthesis of biogenic metallic nanoparticles. Furthermore, these reactions are carried out under ambient conditions (room temperature and atmospheric pressure) and may reduce the toxicity of nanoparticles [1].

Biogenic nanoparticles by microorganisms may be produced via intracellular or extracellular processes, depending on the location where they are formed [2,3]. Extracellular

synthesis has several advantages over intracellular production. It eliminates downstream processing stages, such as sonication, centrifugation, and washing, which are required for the recovery and purification of nanoparticles. Moreover, extracellular peptides, enzymes, reducing cofactors, and organic materials released play a significant role as reducing and natural capping agents [4]. In particular, fungi have the capacity to secrete high quantities of bioactive substances that play a dual functional role as reducing and stabilizing agents for colloidal nanoparticles [5]. Depending on the fungus used, this capping agent may also have biological activity, acting in synergy with the effect of the nanoparticle core [6]. Recently, our group has reported the development of an extracellular cell-free filtrate method for the biological synthesis of silver nanoparticles. Some of these biogenic nanoparticles showed antimicrobial activity against Gram-negative *Escherichia coli* and *Salmonella enterica* bacteria [7,8].

Apart from their widely reported antimicrobial effect on planktonic cells, silver nanoparticles may also eradicate or inhibit microbial biofilm formation, a key virulence factor in many localized chronic infections. Different nanomaterials, non-adhesive, drug-releasing, and contact-killing coatings are under design to prevent biomaterial-associated infection of implants, to penetrate biofilms and to kill multidrug-resistant strains [9,10]. When addressing the control of biofilm infections using nanomaterials, it is key to consider their particle size, shape, and surface properties [11]. Previous studies have shown promising antibiofilm activity of silver nanoparticles, and it was observed that exposure to silver nanoparticles effectively inhibited biofilm formation by Gram-negative *E. coli* and *Pseudomonas aeruginosa* [12]. Moreover, we have recently demonstrated that biogenic silver nanoparticles obtained through the extracellular cell-free extracts of *Phanerochaete chrysosporium*, showed antibiofilm activity against Gram-negative *E. coli* [13]. In spite of this, silver nanoparticles could be prone to aggregation that could lead to a reduced antimicrobial efficacy. To overcome this, natural and environmentally benign compounds may be used as effective stabilizing agents, enhancing bacterial killing in biofilms and reducing the cytotoxicity of silver nanoparticles [10].

In recent years, the application of nisin—a cationic bacteriocin produced by *Lactococcus lactis*—has been extended to the area of biomedicine, in addition to its recognized application as a GRAS food additive with antimicrobial action against Gram-positive bacteria [14]. Nonetheless, the use of bacteriocins has several drawbacks, such as limited antimicrobial spectrum, enzymatic degradation, or binding with other proteins, as well as the development of nisin resistance in bacteria, thus requiring the use of higher doses. To overcome these limitations, conjugation of bacteriocins with metallic nanoparticles offers a promising approach to improve their antimicrobial spectrum. As mentioned earlier, silver nanoparticles have shown antimicrobial activity against Gram-negative bacteria, and hence, it may be useful to increase their antimicrobial effectiveness by combining them with bacteriocins [15]. In particular, it has been shown that electrostatic interactions between negative charges of chemically synthetized metallic nanoparticles and positively charged biomolecules, such as nisin, can lead to the formation of bioconjugates [16]. What is more, different studies have shown that the conjugation of silver nanoparticles with antimicrobial peptides, such as nisin, minimized cytotoxic effects of ionic silver and silver nanoparticles against human cells [17,18].

To the best of our knowledge, no studies have been conducted on the synthesis of nanobioconjugates using microbial nanoparticles and nisin. Therefore, the aim of this work was to synthesize nanobioconjugates by combining silver nanoparticles—obtained from extracellular cell-free extracts of *Phanerochaete chrysosporium*—and nisin, as well as to perform characterization assays (size, morphology, charge, stability, and nisin binding efficiency) and evaluate their antibacterial and antibiofilm properties, in order to improve the antimicrobial potential of these nanomaterials.

2. Materials and Methods

2.1. Materials

Standards and reagents used for the analysis were supplied by Sigma-Aldrich (St. Louis, MO, USA). For the synthesis of stable and high-yield nanoparticles [7], the strain of the fungus *Phanerochaete chrysosporium* CCMG 12G from the Cátedra de Microbiología General Collection CCMG, Facultad de Química, Montevideo, Uruguay was used. *Staphyloccocus aureus* ATCC6538P and *Escherichia coli* ATCC 25922 were used for antimicrobial assays. Culture media were supplied by BD, DIFCO (Franklin Lakes, NJ, USA). Nine-six-well plate (sterilized, 300 µL capacity, MicroWell, NUNC) were supplied by Thermo-FisherScientific, (Waltham, MA, USA). NisinZ® P was purchased from Handary S.A. (Brussels, Belgium). Millipore deionized water was used for solution preparations.

2.2. Methods

2.2.1. Synthesis of Biogenic Silver Nanoparticles (PchNPs)

The mycelia of *Phanerochaete chrysosporium* were grown in Potato Dextrose Agar (PDA) at 28 °C and two plugs of 0.9 cm in diameter were, then, transferred to 500 mL flasks containing 100 mL Potato Dextrose Broth (PDB). Fermentation was carried out at 28 °C, with agitation on an orbital shaker operating at 150 rpm for 72 h. The biomass from cultures was harvested by filtration and, then, washed extensively with sterilized distilled water to remove any remaining media components. Then, synthesis of silver nanoparticles was carried out as described by Sanguiñedo et al. [7]. Wet fungal mycelia were suspended in sterilized distilled water (0.1 g/mL) and incubated with agitation on an orbital shaker operating at 150 rpm. Then, the cell-free filtrate was collected by filtration of this suspension through the membrane filter with 0.45 µm pore size. Finally, 50 mL of the cell-free filtrate was added to 50 mL of a silver nitrate solution. After 24 h incubation in the dark, the absorbance spectrum was measured in the range of 250–800 nm, and the maximum peak was determined. The remaining cell-free filtrate was used as control. After synthesis reaction, the samples were centrifuged at 10,000 rpm for 10 min. The supernatant was removed, and nanoparticles (PchNPs) were washed twice using sterilized distilled water, by centrifuging the nanoparticles for 10 min at 10,000 rpm. The absorbance peak of the purified silver nanoparticles was measured, and the concentration was estimated according to Paramelle et al. [19].

2.2.2. Bioconjugation of Nisin with Biogenic Silver Nanoparticles (PchNPs@nis)

Stock solutions of nisin (0.1 and 0.6 mg/mL) were prepared at 25 °C, using an ultra-pure food grade (>99%) form of Nisin Z and deionized water. Nisin stock solutions were always prepared fresh prior to experiments.

For the preparation of silver nanoparticles–nisin bioconjugates (PchNPs@nis), varying volumes of nisin stock solution were added drop by drop to PchNPs suspensions in microcentrifuge tubes, to obtain final concentrations of 0.135 µg/mL PchNPs and 0, 10, 12, 20, 29, 75, and 150 µg/mL nisin. All samples were incubated overnight in rocker at room temperature. Then, bioconjugates were separated by centrifugation at 10,000 rpm for 45 min at 10 °C [16]. The pellet was washed twice with deionized water, then it was resuspended in 2 mL deionized water and ultrasonicated. The resuspended PchNPs@nis bioconjugates were stored at 4 °C for further analysis, while the supernatant obtained after the first washing cycle—containing the unbound nisin—was kept for the determination of the binding efficiency (BE).

2.2.3. UV-Vis Spectroscopy

The absorbance spectrum was measured in the range of 250–800 nm at predetermined time intervals, using a UV/Vis spectrophotometer (Ultrospec 3100 pro, Amersham Bioscience, Amersham, UK). Additionally, color changes in the reaction mixtures were used as evidence of silver nanoparticles formation.

2.2.4. Particle Size and ζ-Potential

The hydrodynamic diameter and ζ-potential of the PchNPs and PchNPs@nis were determined by dynamic light scattering (DLS) and electrophoretic light scattering (ELS) respectively, using a particle size/zeta potential analyzer (Nano-ZS, Malvern Instruments Ltd., Worcestershire, UK). Samples were prepared at pH 6 in deionized water, and analyses were performed at 25 °C, viscosity of 0.8872 cP, RI of 1.33, and a backscatter angle of 173°. Samples were analyzed in triplicate, and particle size and zeta potential results were expressed as mean ± standard deviations (SD). Results were treated using the Malvern software Zetasizer.

2.2.5. Binding Efficiency

Binding efficiency (BE) of PchNPs@nis bioconjugates was calculated by determining the amount of free nisin found in the supernatant, obtained as described in Section 2.2.2. The BE (%) was calculated using the following equation:

$$BE\ (\%) = \frac{(Nis_t - Nisf)}{Nis_t} \times 100,$$

where Nis_t describes the total amount of nisin used to prepare the bioconjugates, and Nis_f is the amount of nisin in the supernatant.

In order to determine the nisin content of solutions, the colorimetric method bicinchoninic acid (QuantiPro™ BCA Assay Kit, Sigma-Aldrich, St. Louis, MO, USA) was used. Samples and reagents were mixed and heated at 60 °C for 30 min, and the absorbance was measured at 560 nm using a UV/Vis spectrophotometer (Ultrospec 3100 pro, Amersham Bioscience, Amersham, UK). Samples were analyzed in triplicate.

2.2.6. Transmission Electron Microscopy (TEM)

Transmission electron microscopy was performed with an electron microscope (Jem 169 1010, Jeol, Tokyo, Japan) operating at 100 kV, and images were captured with a digital 170 camera (C4742-95, Hamamatsu, Hamamatsu City, Japan). An aliquot of each sample of PchNPs@nis was placed onto a copper grid coated with a holey carbon film and dried at room temperature.

2.2.7. Raman Spectroscopy

Confocal Raman spectroscopy measurements were carried out using a WITec Alpha 300-RA Raman-Confocal Microscope (WITec GmbH, Ulm, Germany). All samples were placed on a glass support. An excitation laser of λ = 532 nm was used, and its power was kept at 10 mW. Each Raman spectrum was obtained by averaging a set of 20–100 spectra of 0.5 s integration time.

2.2.8. Colloidal Stability Assays

The colloidal stability of PchNPs@nis was studied at different pH conditions by the measurement of the absorbance spectrum in the range of 200–800 nm, as reported by Estevez et al. [13].

2.2.9. Antibacterial Activity

Minimal inhibitory concentration (MIC) of the PchNPs, nisin, and PchNPs@nis bioconjugates against *Escherichia coli* and *Staphylococcus aureus* (Supplementary Material) was determined by the microdilution technique, according to the Clinical and Laboratory Standards Institute [20]. In this assay, 100 μL of PchNPs, nisin or PchNPs@nis bioconjugates were added to a 96-well plate containing 100 μL of Mueller Hinton Broth media. The initial solutions of the PchNPs, nisin and PchNPs@nis were prepared in water, and further serial dilutions were performed. Then, wells were supplemented with 100 μL of bacterial suspension (1×10^6 CFU/mL) in Mueller Hinton Broth. A blank sample (bacteria without treatment) was also included in the assay as negative control. The MIC was determined

as the lowest concentration of antimicrobial agent that inhibited the visible growth of a microorganism after 24 h of incubation. A staining of viable cells was carried out with triphenyltetrazolium chloride (TTC).

2.2.10. Antibiofilm Activity

The effect of PchNPs@nis on biofilm formation was examined using a modified microdilution method [21]. Briefly, assays against *S. aureus* biofilms were carried out in a 96-well plate, with four replicates. Serial dilutions of the PchNPs, nisin, and PchNPs@nis in nutrient broth were deposited, and a bacterial suspension (1×10^8 cells/mL) was added. Control wells containing sterile nutrient broth (sterile control, SC) and nutrient broth + sterile water + bacterial suspension (non-treated biofilm, NTB) were included. The plate was incubated at 37 °C for 24 h.

After the supernatant was removed, the wells were washed with distilled water and dried at 50 °C for 40 min. Then, the attached cells were stained with 1% crystal violet dye. The crystal violet dye was resuspended in ethanol: acetone (70:30), and the absorbance of the solution was measured at 590 nm. The absorbance measurements of each sample, extracts, NTB, and SC were compared, and the inhibition percentage was calculated. The amount of formed biofilm was expressed in biofilm biomass unit (BBU), which was arbitrarily defined as 0.1 OD590 equal to 1 BBU [22]. The minimal biofilm inhibitory concentration (MBIC) was defined as the minimal concentration able to inhibit at least 90% of the biofilm formation.

Statistical Analysis

Experiments were performed at least in quadruplicate, and the averages and standard deviations were calculated for all experiments. Results were plotted as means values with error bars that represent standard deviations. Data were statistically analyzed using ANOVA and a post hoc Tukey test for multiple comparisons (p value < 0.05).

3. Results and Discussion

3.1. PchNPs@nis Nanobioconjugates with Antibiofilm Activity

3.1.1. Synthesis and Characterization of PchNPs@nis

UV-Vis Spectra

After 24 h reaction of synthesis reaction, the absorbance spectrum was measured in the range of 250–800 nm and the maximum peak was determined. Color change in the reaction mixture as well as the presence of an absorption band between 400 and 450 nm—which corresponds to the surface plasmon resonance (SPR)—confirmed the formation of the biogenic silver nanoparticles, PchNPs. After purification, the UV-Vis spectra of PchNps showed an absorption band at 440 nm, corresponding to the SPR band of silver nanoparticles and coincident with previously reported results [13].

Upon addition of nisin and purification, PchNPs@nis bioconjugates were formed with a final PchNPs concentration of 0.135 μg/mL and a final nisin concentration of 10 μg/mL. UV-Vis spectra of the PchNPs and PchNPs@nis were obtained. As shown in Figure 1, both spectra showed similar peak positions and intensities, suggesting that binding of nisin did not cause the aggregation of PchNPs at the evaluated concentration.

Particle Size

Figure 2 presents the results of DLS characterization of PchNPs and PchNPs@nis. PchNPs showed one single population with a hydrodynamic diameter of 45.34 (17.44) nm (Figure 2a), in good agreement with previous findings that reported the formation of biogenic silver nanoparticles with a hydrodynamic diameter of ca. 45 nm [13].
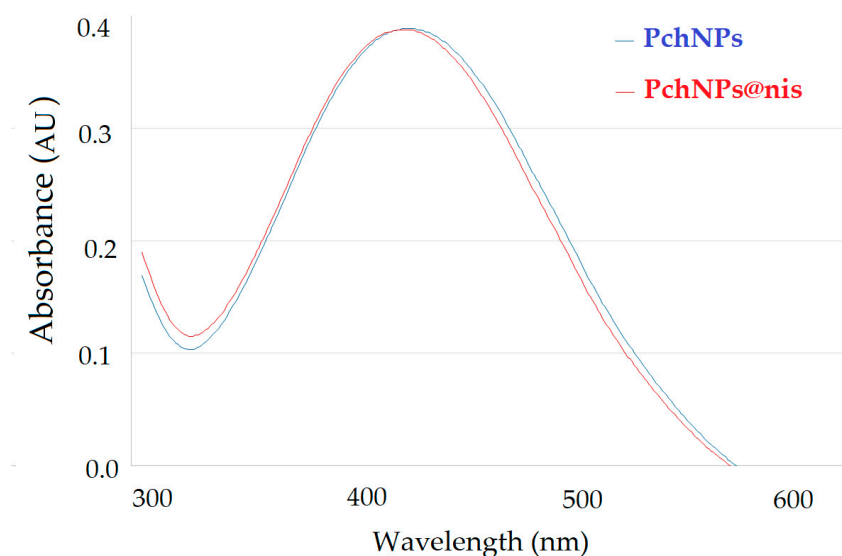
Figure 1. UV-visible absorption spectra showing the SPR band of PchNPs and PchNps@nis.
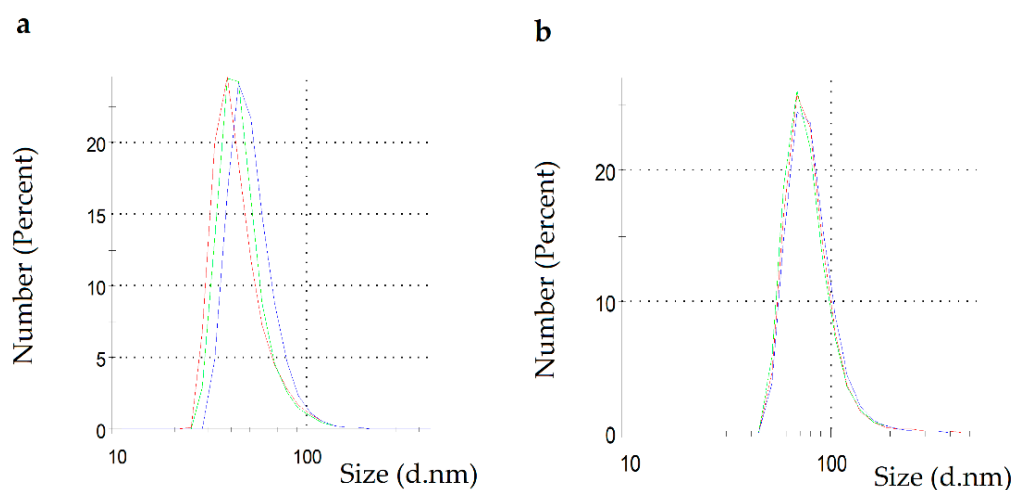

Figure 2. DLS measurement: (**a**) PchNPs and (**b**) PchNPs@nis.

As expected, PchNPs@nis showed a higher diameter of 62.29 (26.17) nm, probably due to the conjugation of the biogenic nanoparticles with nisin (Figure 2b). Previous studies also showed an increase in the average size of silver nanoparticles upon assembly of nisin [16,23]. Moreover, the PDI value of this system (0.382) was lower than 0.4, indicating a moderately polydisperse distribution [24].

ζ-Potential

ζ-potential determination showed that PchNPs (Figure 3a) and PchNPs@nis (Figure 3b) had negative zeta potential values of −23.2 (3.9) and −27.0 (5.4) mV, respectively, indicating a net negative surface charge. These results were consistent with a previous study by Estevez et al. that reported that PchNPs had a zeta potential value of −24.8 mV [13]. Moreover, these absolute values were close to the accepted threshold for stability (| zeta potential | > 30 mV) and did not exhibit precipitation, suggesting their colloidal stability in aqueous media [25].
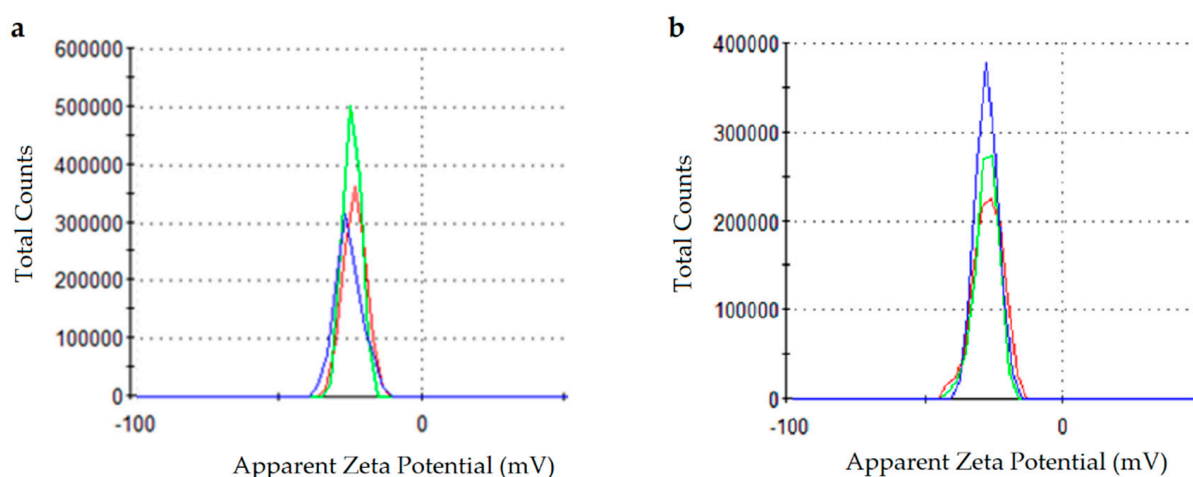
Figure 3. ζ-potential measurements: (**a**) PchNPs and (**b**) PchNPs@nis.

Colloidal Stability Assays

To further investigate the colloidal stability of PchNPs@nis, SPR spectra were obtained from samples at pH 4 and 8 (Figure 4). Aggregation of nanoparticles generates a decrease in intensity of the SPR band as well as a shift in the visible spectrum towards the infrared [7]. According to this, the results showed that PchNPS@nis were stable at the evaluated pH conditions, since no shifts in the position of the SPR band were observed when nisin was added to PchNPs.

Figure 4. Stability of PchNPs and PchNPs@nis at (**a**) pH 4 and (**b**) pH 8.

3.1.2. Biological Activity

The ability of different PchNP concentrations to inhibit the *S. aureus* biofilm formation was evaluated (Figure 5). It can be observed that, although there was a decrease in biofilm formation when PchNPs with the highest concentration (0.075 µg/mL) were applied, the difference was not significant. However, biofilm formation was stimulated for concentrations above 0.038 µg/mL. These results were in line with previous studies, which reported the stimulation of biofilm growth at subinhibitory concentrations [26].
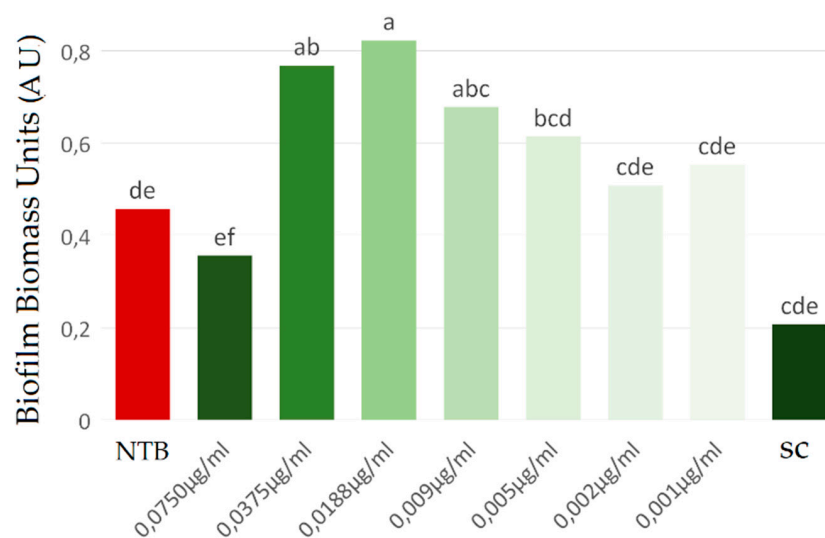
Figure 5. Evaluation of the inhibition of *Staphylococcus aureus* biofilm by PchNPs at different concentrations. NTB: non-treated biofilm, SC: sterile control. Different letters (a,b,c,d,e,f) represent significant differences at $p < 0.05$ probability level, according to ANOVA and Tukey's test.

Next, the antibiofilm activity of nisin and PchNPs@nis bioconjugates was investigated. Bioconjugates were capable of significantly inhibiting biofilms when used at concentrations of 0.036, 0.018, and 0.009 µg/mL PchNPs, which correspond to 1/4, 1/8, and 1/16 PchNPs@nis dilutions, respectively (Figure 6). Similarly, Zhao and Kuipers observed that silver–nisin nanoparticles prepared by microwave-assisted synthesis showed a strong antibiofilm activity against *S. aureus* [17]. The MBIC, defined as the lowest concentration of antimicrobial agent required to inhibit at least 90% of the biofilm growth, was also determined for the PchNPs@nis and had a value of 0.018 µg/mL. Besides, as can be observed in Figure 6, unconjugated nisin did not inhibit biofilm formation at the equivalent nisin concentrations studied in the bioconjugates (0.31–2.50 µg/mL).
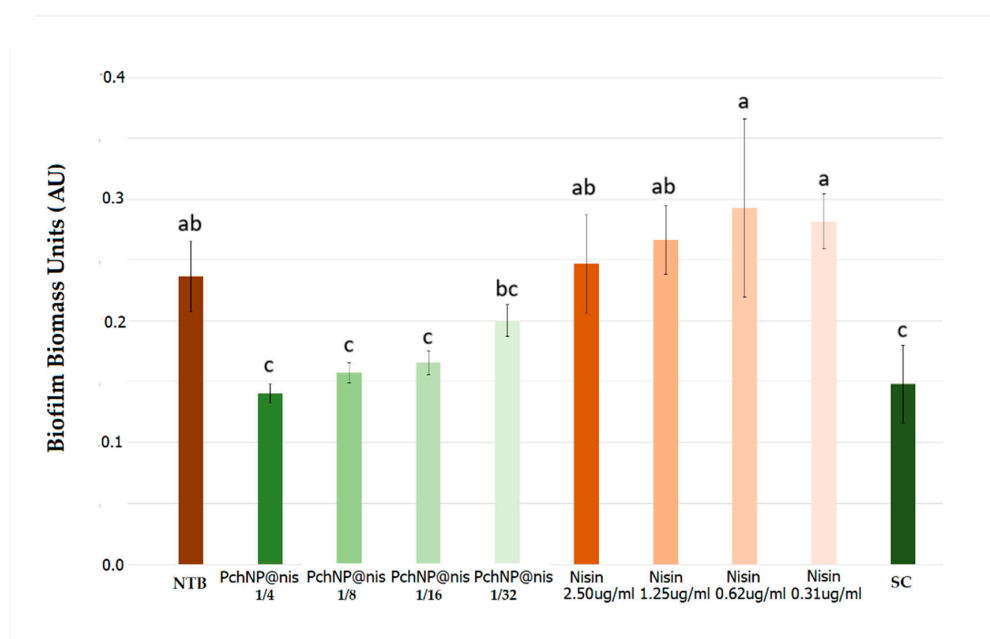

Figure 6. Evaluation of the inhibition of *Staphylococcus aureus* biofilm by PchNPs@nis and nisin at different concentrations. NTB: non-treated biofilm, SC: sterile control. Different letters (a,b,c) represent significant differences at $p < 0.05$ probability level, according to ANOVA and Tukey's test.

As a result, the antibiofilm assays revealed that while neither of the two unconjugated antimicrobials were capable of inhibiting biofilm formation by *S. aureus*, PchNPs@nis bioconjugates effectively prevented biofilm growth by that microorganism.

Antibacterial assays were performed to investigate the antimicrobial effect of these bio-conjugates against *S. aureus* planktonic cells, but no enhanced inhibition was observed, and thus, we hypothesized that the content of bound nisin in the PchNPs@nis was not sufficient to produce a significant enhanced antibacterial effect. Therefore, bioconjugates with higher nisin concentrations were prepared and tested as described in the following sections.

3.2. PchNPs@nis Bioconjugates with Antimicrobial Activity Againts Gram-Positive and Gram-Negative Bacteria

3.2.1. Characterization of PchNPs@nis Bioconjugates Synthetized under Different Conditions

PchNPs@nis bioconjugates (0.0675 µg/mL PchNPs) with greater nisin content were prepared, reaching final nisin concentrations of 12, 20, 29, 75, and 150 µg/mL. Particle size and ζ-potential measurements were conducted in order to find the suitable range of nisin content for the formation of stable PchNPs@nis nanobioconjugates. With increasing nisin content, ζ-potential results shifted to more positive values (reaching ca. -13 mV) (Figure 7), due to the increasing contribution of the positively charged groups of nisin to the overall surface charge. Pandit et al. also observed that after the incorporation of nisin onto silver nanoparticles, zeta potential values of the bioconjugates increased [23]. Moreover, Arakha et al. studied nisin–silver bioconjugates prepared with commercial silver nanoparticles and found that these results stemmed from electrostatic interactions between cationic and anionic surfaces, providing further evidence of the conjugation of nisin onto the biogenic PchNPs interface [16].
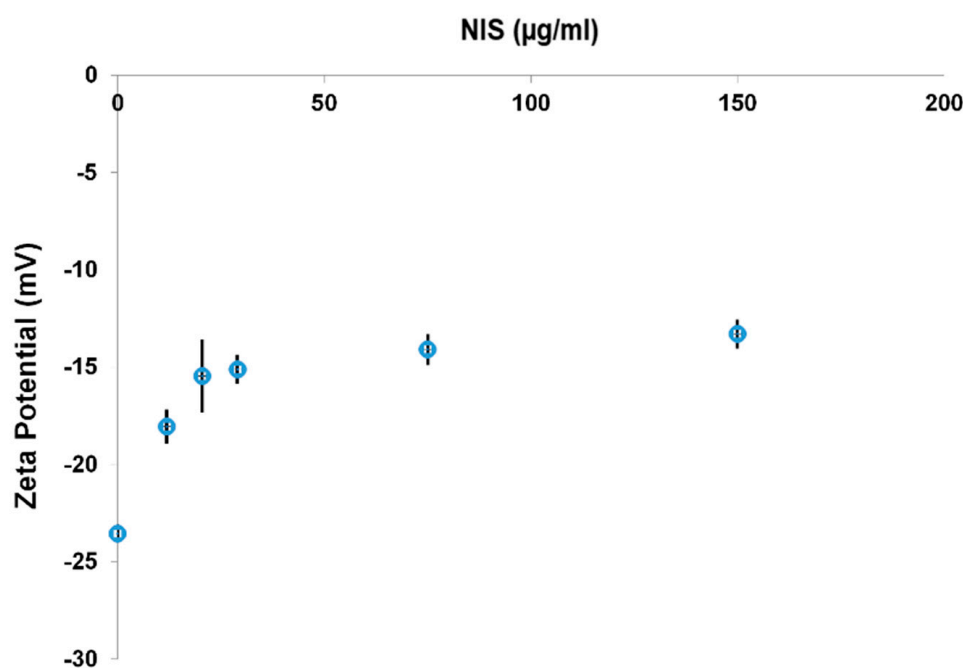

Figure 7. ζ-potential measurements of PchNPs@nis with increasing nisin content.

Furthermore, particle size determinations (Figure 8) showed that the hydrodynamic diameter of bioconjugates increased with higher nisin concentration. Bioconjugates with lower nisin concentrations (12–29 µg/mL) had particle size values that ranged between ca. 60 and 130 nm. On the other hand, PchNPs@nis bioconjugates prepared with higher nisin content presented particle size values above 1000 nm. Therefore, higher nisin con-centrations led to the formation of unstable particles and aggregates, due to a partial neutralization of the nanoparticles surface charge upon nisin binding, consistent with ζ-

potential results. The electrostatic repulsive forces between surface charges of nanoparticles play an important role in stability; nanoparticle suspensions that show net potential close to neutrality, probably aggregate, losing their size-dependent properties as nanomaterials [27].
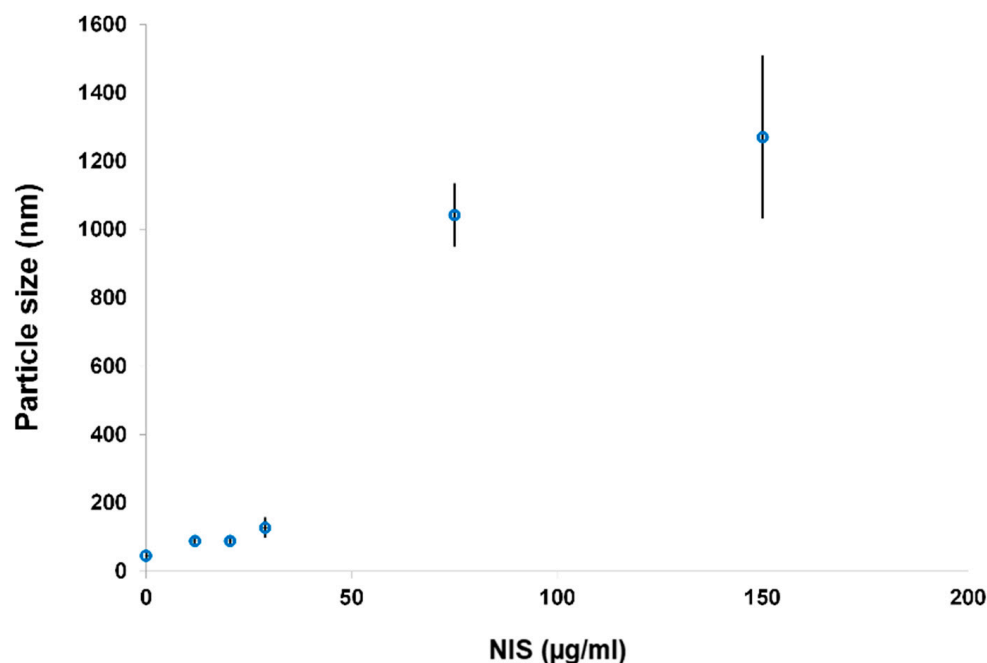

Figure 8. Particle size measurements of PchNPs@nis with increasing nisin content.

Binding efficiency (BE) was determined in systems that had the desired stability and size properties, namely PchNPs@nis with lower nisin content (12, 20, and 29 µg/mL). As can be observed in Table 1, resulting BE values were higher than 75% and increased with decreasing nisin content. For PchNPs@nis bioconjugates with 12 µg/mL, the BE percentage was ca. 100%, suggesting an excellent affinity of nisin to the biogenic PchNPs.

Table 1. Binding efficiency (BE) of PchNPs@nis.

Nisin Concentration (µg/mL)	BE (%)
12	100 (5.8)
20	95.9 (3.5)
29	76.1 (1.1)

Furthermore, complementary characterization assays of these PchNPs@nis were carried out using UV-Vis, transmission electron microscopy (TEM) and Raman spectroscopy. As seen in Figure 9a, the UV-Vis spectrum was similar to the spectrum of unconjugated PchNPs, with an absorption band at ca. 440 nm ascribable to SPR. This result suggests that binding of nisin did not cause the aggregation of PchNPs at the evaluated nisin concentration, as explained in Section 3.1.1.

Next, Raman spectroscopy was used to characterize the surface functional groups of the PchNPs@nis nanobioconjugates (Figure 9b). The Raman spectra of the bioconjugates, displayed bands that could be attributed to nisin but not to the nanoparticles, e.g., the band close to 1700 cm^{-1}, supporting the incorporation of nisin onto the surface of the nanoparticle. This result is in line with the FTIR analysis reported by Zhao and Kuipers to verify Ag–nisin nanoparticle formation, showing the characteristic peak of nisin at 1658.45 cm^{-1}, (corresponding to a C–O stretching of amide I), detected in Ag–nisin nanoparticles [17].
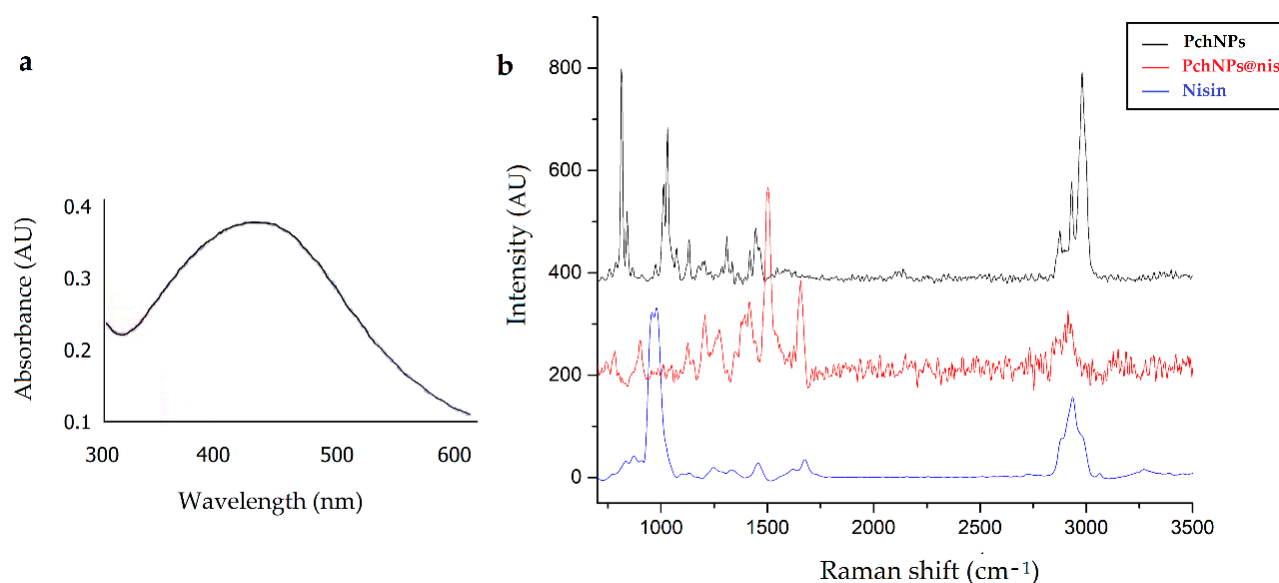
Figure 9. UV-Vis (**a**) and Raman (**b**) spectra of nanobioconjugates PchNPs@nis.

Additionally, the Raman spectra of PchNPs@nis showed differences in intensities, shifts, or the appearance of new Raman bands when compared to the spectra of unconjugated nisin and PchNPs. Specifically, differences were found in the bands at 1474, 1443, 1298, 1022, 1100, 1011, 845, and 815 cm^{-1}. This is an important region, since, as shown in the study by Estevez et al. [13], these bands could be attributed to the presence of the amino acids L-alanine and L-valine involved in the capping of the biogenic PchNPs. Likewise, the PchNPs@nis and nisin spectrum revealed changes in the positions and intensity ratio of bands that could be ascribed to the vibrational modes of amide I at ca. 1676 cm^{-1} (shifted to 1657 cm^{-1}), amide III at ca. 1245 cm^{-1} (shifted to 1206 cm^{-1}), to anti-symmetric deformations of side peptide chains, e.g., at ca. 1425 cm^{-1} (shifted to 1415 cm^{-1}), 1450 cm^{-1} (disappeared), and 1475 cm^{-1} (disappeared), and also an intense band displayed at 1504 cm^{-1}. Furthermore, in the present work, the PchNPs@nis showed a significant decrease in the Raman band at ca. 1000 cm^{-1} that could be ascribed to stretching vibrations of C–C, suggesting that the formation of the bioconjugate might restrict the mobility of the aliphatic chain of the lysine residue of nisin [28,29]. In sum, the Raman analysis revealed changes in the spectra of PchNPs@nis that could stem from molecular interactions between the amino acids present in the capping of the biogenic PchNPs and nisin, suggesting the formation of the PchNPs@nis nanobioconjugates.

Finally, the TEM characterization showed that the nanobioconjugates PchNPs@nis were spherical and with an average size (which corresponds to the metallic core of the silver nanoparticles) ca. 20–40 nm (Figure 10). These results are coincident with size values and morphology reported by Estevez et al. for these biogenic nanoparticles [8].

3.2.2. Antimicrobial Activity of Stable PchNPs@nis Nanobioconjugates

The antimicrobial activity of unconjugated nisin, PchNPs, and stable PchNPs@nis nanoconjugates was evaluated through MIC determination against *S. aureus* and *E. coli*. A decrease in MIC values was only observed upon application of bioconjugates with the highest content of nisin (29 µg/mL), and the corresponding results are shown in Table 2.
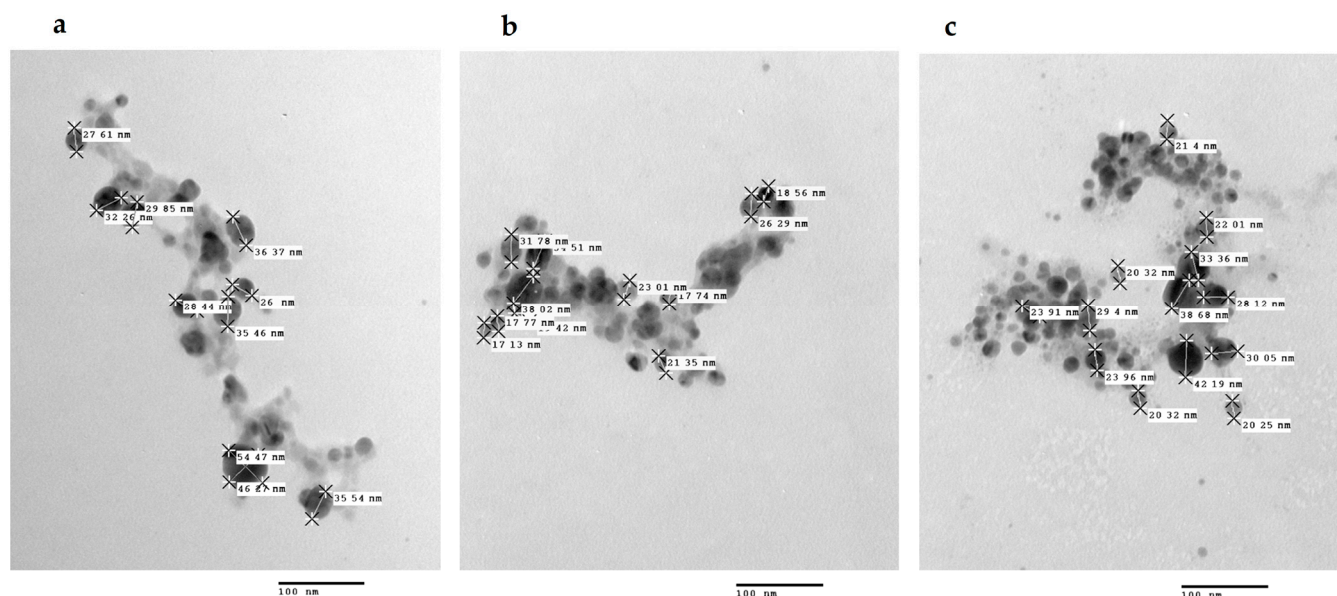
Figure 10. TEM images of the PchNPs@nis nanobioconjugates. Nisin concentrations: (**a**) 12 (µg/mL), (**b**) 20 (µg/mL), (**c**) 29 (µg/mL).

Table 2. MIC of PchNPs and PchNPs@nis against Gram-positive *S. aureus* and Gram-negative *E. coli*.

Microorganism	MIC PchNPs	MIC Nisin	MIC PchNPs@nis
E. coli	0.017 µg/mL	156 µg/mL	0.017 µg/mL
S. aureus	0.068 µg/mL	0.150 µg/mL	0.017 µg/mL

Unconjugated nisin displayed the highest MIC value (156 µg/mL) against *E. coli*. This result was expected, since nisin has been shown to be an active antimicrobial agent against Gram-positive but not Gram-negative bacteria [14]. On the other hand, PchNPs@nis presented a MIC value of 0.017 µg/mL against *S. aureus*, showing that PchNPs@nis were more effective than the unconjugated antimicrobial tested inhibiting *S. aureus* growth.

In line with these results, Zhao and Kuipers [17] also demonstrated that silver–nisin nanoparticles showed antimicrobial activity against *S. aureus* and *E. coli*. However, MIC values reported in their study (4 and 2 µg/mL, respectively) were higher than the values presented in this study. This could be explained by the fact that biogenic nanoparticles contain capping agents that can result in better antimicrobial activity [30] than that of silver nanoparticles prepared using a microwave-assisted method. In addition to this, Pandit et al. also showed that the antimicrobial potential of nisin increased after bioconjugation with silver nanoparticles [23].

Therefore, these results show that PchNPs@nis nanoconjugates were capable of broadening the spectrum of action of the unconjugated PchNPs or nisin, enhancing their antimicrobial activity against two different bacteria that may cause severe diseases, such as Gram-positive *Staphylococcus aureus* and Gram-negative *Escherichia coli* [31].

For the application of new antimicrobial or antibiofilm nanomaterials, it is necessary to evaluate their toxicity. Previous studies carried out with biogenic silver nanoparticles have shown that, in addition to providing greater antimicrobial activity, stabilizing agents (capping) may reduce cytotoxicity and genotoxicity of nanoparticles [30]. Furthermore, different studies with nisin have shown no toxicity evidence, supporting human therapeutic applications of this peptide [32,33]. According to Zhao and Kuipers [17], human cells were unaffected by the presence of nisin at 128 µg/mL, and they also reported that silver–nisin nanoparticles prepared by microwave-assisted synthesis showed lower cytotoxicity than clinically used ionic silver. Therefore, in the present study, it can be expected that the nanobioconjugates studied (nisin concentration < 50 ug/mL) display an acceptable safety

profile. However, future studies should include the toxicity assessment of PchNps@nis nanobioconjugates on non-tumor cell lines.

4. Conclusions

Nanobioconjugates were produced by combining biogenic silver nanoparticles—obtained from extracellular cell-free extracts of *Phanerochaete chrysosporium*—and bacteriocin nisin. UV-Vis analyses confirmed the formation of the biogenic silver nanoparticles and showed that bound nisin did not cause aggregation of nanoparticles. The particle size of PchNPs@nis increased with higher nisin concentration and zeta potential turned to more positive values due to the incorporation of positively charged nisin. Additionally, nisin showed an excellent affinity to the bioconjugates as displayed by the high BE values (75–100%) obtained. Characterization by Raman spectroscopy and TEM imaging provided further evidence of formation of bioconjugates. Stable synthesized PchNPs@nis were not only able to inhibit the formation of *S. aureus* biofilm, but also showed a broad spectrum of action inhibiting the planktonic cell growth of Gram-positive and Gram-negative bacteria. In conclusion, we successfully developed PchNPs@nis with promising properties for their application as potential antimicrobial nanomaterials.

References

1. Gour, A.; Jain, N.K. Advances in green synthesis of nanoparticles. *Artif. Cells Nanomed. Biotechnol.* **2019**, *47*, 844–851. [CrossRef]
2. Alamri, S.A.M.; Hashem, M.; Nafady, N.A.; Sayed, M.A.; Alshehri, A.M.; Alshaboury, G. Controllable biogenic synthesis of intracellular silver/silver chloride nanoparticles by *Meyerozyma guilliermondii* KX008616. *J. Microbiol. Biotechnol.* **2018**, *28*, 917–930. [CrossRef]
3. Javani, S.; Marín, I.; Amils, R.; Abad, J.P. Four psychrophilic bacteria from Antarctica extracellularly biosynthesize at low temperature highly stable silver nanoparticles with outstanding antimicrobial activity. *Colloids Surf. A Physicochem. Eng. Asp.* **2015**, *483*, 60–69. [CrossRef]
4. Khan, M.R.; Fromm, K.M.; Rizvi, T.F.; Giese, B.; Ahamad, F.; Turner, R.J.; Füeg, M.; Marsili, E. Metal nanoparticle-microbe interactions: Synthesis and antimicrobial effects. *Part. Part. Syst. Charact.* **2019**, *37*, 1900419. [CrossRef]

5. Neethu, S.; Midhun, S.J.; Radhakrishnan, E.K.; Jyothis, M. Surface functionalization of central venous catheter with mycofabricated silver nanoparticles and its antibiofilm activity on multidrug resistant *Acinetobacter baumannii*. *Microb. Pathog.* **2020**, *138*, 103832. [CrossRef]

6. Guilger-Casagrande, M.; de Lima, R. Synthesis of silver nanoparticles mediated by Fungi: A review. *Front. Bioeng. Biotechnol.* **2019**, *7*, 287. [CrossRef]

7. Sanguiñedo, P.; Fratila, R.M.; Estevez, M.B.; Martínez de la Fuente, J.; Grazú, V.; Alborés, S. Extracellular biosynthesis of silver nanoparticles using fungi and their antibacterial activity. *Nano Biomed. Eng.* **2018**, *10*, 156–164. [CrossRef]

8. Estevez, M.B.; Casaux, M.L.; Fraga, M.; Faccio, R.; Alborés, S. Biogenic silver nanoparticles as a strategy in the fight against multi-resistant salmonella enterica isolated from dairy calves. *Front. Bioeng. Biotechnol.* **2021**, *9*, 314. [CrossRef]

9. Pipattanachat, S.; Qin, J.; Rokaya, D.; Thanyasrisung, P.; Srimaneepong, V. Biofilm inhibition and bactericidal activity of NiTi alloy coated with graphene oxide/silver nanoparticles via electrophoretic deposition. *Sci. Rep.* **2021**, *11*, 14008. [CrossRef]

10. Castillo, H.A.P.; Castellanos, L.N.M.; Chamorro, R.M.; Martínez, R.R.; Borunda, E.O. Nanoparticles as new therapeutic agents against candida albicans. *Candida Albicans* **2018**. [CrossRef]

11. Singh, P.; Pandit, S.; Beshay, M.; Mokkapati, V.R.S.S.; Garnaes, J.; Olsson, M.E.; Sultan, A.; Mackevica, A.; Mateiu, R.V.; Lütken, H.; et al. Anti-biofilm effects of gold and silver nanoparticles synthesized by the *Rhodiola rosea* rhizome extracts. *Artif. Cells Nanomed. Biotechnol.* **2018**, *46*, S886–S899. [CrossRef]

12. Salar, R.; Kumar, R.; Prasad, M.; Brar, B.; Nain, V. Green synthesis of silver nanoparticles and its applications—A review. *Nano Trends-A J. Nanotechnol. Appl.* **2017**, *19*, 1–22.

13. Estevez, M.B.; Raffaelli, S.; Mitchell, S.G.; Faccio, R.; Alborés, S. Biofilm eradication using biogenic silver nanoparticles. *Molecules* **2020**, *25*, 2023. [CrossRef] [PubMed]

14. Andre, C.; de Jesus Pimentel-Filho, N.; de Almeida Costa, P.M.; Vanetti, M.C.D. Changes in the composition and architecture of staphylococcal biofilm by nisin. *Braz. J. Microbiol.* **2019**, *50*, 1083–1090. [CrossRef]

15. Sulthana, R.; Archer, A.C. Bacteriocin nanoconjugates: Boon to medical and food industry. *J. Appl. Microbiol.* **2021**, *131*, 1056–1071. [CrossRef]

16. Arakha, M.; Borah, S.M.; Saleem, M.; Jha, A.N.; Jha, S. Interfacial assembly at silver nanoparticle enhances the antibacterial efficacy of nisin. *Free Radic. Biol. Med.* **2016**, *101*, 434–445. [CrossRef]

17. Zhao, X.; Kuipers, O.P. Synthesis of silver-nisin nanoparticles with low cytotoxicity as antimicrobials against biofilm-forming pathogens. *Colloids Surf. B Biointerfaces* **2021**, *206*, 111965. [CrossRef] [PubMed]

18. Liu, L.; Yang, J.; Xie, J.; Luo, Z.; Jiang, J.; Yang, Y.Y.; Liu, S. The potent antimicrobial properties of cell penetrating peptide-conjugated silver nanoparticles with excellent selectivity for Gram-positive bacteria over erythrocytes. *Nanoscale* **2013**, *5*, 3834–3840. [CrossRef]

19. Paramelle, D.; Sadovoy, A.; Gorelik, S.; Free, P.; Hobley, J.; Fernig, D.G. A rapid method to estimate the concentration of citrate capped silver nanoparticles from UV-visible light spectra. *Analyst* **2014**, *139*, 4855–4861. [CrossRef]

20. CLSI. Methods for dilution antimicrobial susceptibility tests for bacteria that grow aerobically. In *Approved Standard*, 10th ed.; CLSI: Wayne, PA, USA, 2015; p. 35.

21. Teanpaisan, R.; Kawsud, P.; Pahumunto, N.; Puripattanavong, J. Screening for antibacterial and antibiofilm activity in Thai medicinal plant extracts against oral microorganisms. *J. Tradit. Complementary Med.* **2017**, *7*, 172–177. [CrossRef]

22. Marioni, J.; Bresolí-Obach, R.; Agut, M.; Comini, L.R.; Cabrera, J.L.; Paraje, M.G.; Nonell, S.; Núñez Montoya, S.C. On the mechanism of Candida tropicalis biofilm reduction by the combined action of naturally-occurring anthraquinones and blue light. *PLoS ONE* **2017**, *12*, e0181517. [CrossRef]

23. Pandit, R.; Rai, M.; Santos, C.A. Enhanced antimicrobial activity of the food-protecting nisin peptide by bioconjugation with silver nanoparticles. *Environ. Chem. Lett.* **2017**, *15*, 443–452. [CrossRef]

24. Bhattacharjee, S. DLS and zeta potential—What they are and what they are not? *J. Control. Release* **2016**, *235*, 337–351. [CrossRef]

25. Uskoković, V. Dynamic light scattering based microelectrophoresis: Main prospects and limitations. *J. Dispers. Sci. Technol.* **2012**, *33*, 1762–1786. [CrossRef]

26. Ranieri, M.R.; Whitchurch, C.B.; Burrows, L.L. Mechanisms of biofilm stimulation by subinhibitory concentrations of antimicro-bials. *Curr. Opin. Microbiol.* **2018**, *45*, 164–169. [CrossRef]

27. Joseph, E.; Singhvi, G. Chapter 4—Multifunctional nanocrystals for cancer therapy: A potential nanocarrier. In *Nanomaterials for Drug Delivery and Therapy*; Grumezescu, A.M., Ed.; William Andrew Publishing: Burlington, MA, USA, 2019; pp. 91–116.

28. Zimet, P.; Mombrú, Á.W.; Faccio, R.; Brugnini, G.; Miraballes, I.; Rufo, C.; Pardo, H. Optimization and characterization of nisin-loaded alginate-chitosan nanoparticles with antimicrobial activity in lean beef. *LWT* **2018**, *91*, 107–116. [CrossRef]

29. Kuhar, N.; Sil, S.; Umapathy, S. Potential of Raman spectroscopic techniques to study proteins. *Spectrochim. Acta Part A Mol. Biomol. Spectrosc.* **2021**, *258*, 119712. [CrossRef]

30. Guilger-Casagrande, M.; Germano-Costa, T.; Bilesky-José, N.; Pasquoto-Stigliani, T.; Carvalho, L.; Fraceto, L.F.; de Lima, R. Influence of the capping of biogenic silver nanoparticles on their toxicity and mechanism of action towards *Sclerotinia sclerotiorum*. *J. Nanobiotechnol.* **2021**, *19*, 53. [CrossRef]

31. Predoi, D.; Iconaru, S.L.; Buton, N.; Badea, M.L.; Marutescu, L. Antimicrobial activity of new materials based on lavender and basil essential oils and hydroxyapatite. *Nanomaterials* **2018**, *8*, 291. [CrossRef]

32.   Shin, J.M.; Ateia, I.; Paulus, J.R.; Liu, H.; Fenno, J.C.; Rickard, A.H.; Kapila, Y.L. Antimicrobial nisin acts against saliva derived
        multi-species biofilms without cytotoxicity to human oral cells. *Front. Microbiol.* **2015**, *6*, 617. [CrossRef]
33.   Gupta, S.; Reddy, K. Evaluation of developmental toxicity of microbicide Nisin in rats. *Food Chem. Toxicol.* **2008**, *46*, 598–603.
        [CrossRef]